Detunable Transverse Electromagnetic (TEM) Volume Coil for High-Field NMR

J.T. Vaughan,* G. Adriany, M. Garwood, E. Yacoub, T. Duong, L. DelaBarre, P. Andersen, and K. Ugurbil

Most high-field MRI systems do not have the actively detuned body coils that are integral to clinical systems operating at 1.5T and lower field strengths. Therefore, many clinical applications requiring homogeneous volume excitation in combination with local surface coil reception are not easily implemented at high fields. To solve this problem for neuroimaging applications, actively detunable transverse electromagnetic (TEM) head coils were developed to be used with receive-only surface coils for signal-to-noise ratio (SNR) gains and improved spatial coverage from homogeneously excited regions. These SNR and field of view (FOV) gains were achieved by application of a detunable TEM volume coil to human brain imaging at 4T. Magn Reson Med 47:990–1000, 2002. © 2002 Wiley-Liss, Inc.
Key words: high-field MRI; RF volume coil; TEM coil; detuning

In the last decade, MRI studies conducted at 3T and 4T have demonstrated the utility of high magnetic fields in functional, anatomical, and metabolic imaging of the human brain (1–5). To date, high-field imaging has relied almost exclusively on the use of head coils for acquiring homogeneous images, or on surface coils for high-sensitivity images from a limited volume in the region of interest (ROI). At fields lower than 3T, however, clinicians and researchers often prefer to combine the use of a "body" coil for homogeneous spin excitation and a surface coil for high signal-to-noise ratio (SNR) reception from a localized ROI. Due to the dearth of actively detunable body coils for high-field systems, however, this option of using homogeneous transmit coils together with sensitive receive coils has not been available for high-field studies, especially for those at 4T and above. For brain imaging, a solution to this problem is presented in the form of a detunable head coil with a diameter sufficiently large to accommodate surface coils placed about the head of a subject.

In the combined use of a body coil and a surface coil for RF transmission and signal reception, respectively, the transmit coil must be electronically (actively) detuned from the Larmor frequency during signal reception. The surface coil must be actively detuned during RF transmission for signal excitation. In the absence of a homogeneous volume transmitter, a surface coil is used for both transmit and receive functions when high sensitivity is required. The inhomogeneous B_1 profile of the surface coil, however, leads to a nonuniform excitation profile. Sensitivity of detection by the surface coil is similarly nonuniform since the sensitivity of the coil at a given location in space is proportional to the B_1 field generated at that location. This nonuniform B_1 profile results in a rapidly decaying signal intensity with increasing distance from the surface coil. In many imaging applications, undesirable spatial variations in tissue contrast result. While this problem can be addressed to a degree with adiabatic excitation and refocusing pulses, this approach narrows the available choices of imaging and spectroscopy sequences that can be employed. While slice-selective refocusing can be achieved adiabatically (6–8), slice-selective excitation is more difficult. Although a slice-selective adiabatic excitation pulse exists (9), the utility of this pulse is limited to animal experiments in which higher RF powers can be used. Consequently, rapid multislice imaging of humans is not currently practical with adiabatic RF pulses.

Transmit/receive (T/R) phased-array coils have been proposed as an alternative means of achieving homogeneous transmission and high-sensitivity reception at high fields (10). However, the preferred method for combining the data from phased-array coils by optimizing the sensitivity at each pixel in the image is not available when the array is used for both transmission and reception. When used as a transmit coil, the phased array requires combination of the data using far-field, phased-array techniques (global phase shifters and gains applied to the analog signals). However, the relative gains and phases between the receivers of the arrays can vary dramatically as a function of position in the image. Therefore, when phased arrays are used as T/R coils, combining the analog signals with a global gain and phase shift can optimize the SNR in a limited region only.

Thus, while there are clear advantages to using large circumscribing volume coils for excitation and surface coils for detection, this approach presents the challenge of building an *efficient* head or body coil for the highest magnetic fields. The building of such coils is not a matter of simply retuning conventional 64 MHz coils. In addition to the tuning difficulties of large inductive coils, RF coil circuits longer than 1/10 λ begin to radiate a significant portion of their energy as an antenna. These radiation losses subtract energy from the RF coil's B_1 field, and add energy ultimately as heat and noise signal to the subject and magnet bore environment. At 3T and higher, radiation losses can limit the safe and effective use of an improperly designed head or body coil, even if the coil achieves resonance at the higher Larmor frequency. By means of simplified analysis, the following paragraphs describe the nature of losses common to high-frequency coils, and approaches to limit these losses. A more rigorous accounting

of the losses discussed will require full wave numerical analyses, which will be pursued in a future study.

High-Frequency Coil Losses

Increased SNR is sought by making NMR measurements at higher B_0 magnetic fields. However, magnetic field strength is only one of several parameters affecting the NMR SNR. RF coil and tissue losses can significantly limit the potential SNR gains to be realized at higher field strengths. SNR (and transmit efficiency) will suffer when any one of the parameters in the following proportionality is not optimized (11).

$$\text{SNR} \propto (\omega^2 B_1)/\sqrt{(R_\Omega + R_r + R_{tissue})} \qquad [1]$$

R_Ω, R_r, and R_{tissue} are the coil's ohmic resistance, radiation resistance, and coupled tissue losses, respectively.

Tissue losses begin to degrade the SNR at higher Larmor frequencies (12). In the head, losses to the tissue conductor R_σ are approximately proportional to the Larmor frequency ω. Losses to the tissue dielectric R_ϵ, are approximately proportional to ω^2 (13). These conductive and dielectric losses represented by R_{tissue} in Eq. [1] are limited in practice by using local surface coils or array coils efficiently and exclusively coupled to the ROI.

In addition to reactive tissue loading, RF losses in the coil also become significant at higher frequencies. In Eq. [1] the resistive loss of the RF coil increases with frequency as $\sqrt{\omega}$ (Eq. [2]), and the radiation losses R_r increase as ω^4 (Eq. [3]). The radiation losses also increase as the coil size increases as S^2, where S is the area bounded by a unit cross-section of the coil.

$$R_\Omega = R_s(\ell/w) \qquad [2]$$

$$\text{for, } R_s = \sqrt{(\omega\mu/2\sigma)} = 1/\sigma\delta$$

R_s is the skin resistance at one skin depth, δ of an RF circuit of length l, and width w.

$$R_r = 20(\beta^2 S)^2$$

$$\approx 31{,}200(S/\lambda^2)^2 \quad \text{(for a coil of arbitrary S)} \quad [3]$$

β is the free space phase constant for an RF circuit resonant at $f = c/\lambda$ (14).

These equations shed light on the ongoing challenge to build efficient body coils whose high-frequency (high-field) circuit dimensions can assume large fractions of a wavelength. From Eqs. [1] and [3], it is clear that uncontrolled radiative losses become severe to the point of limiting and eventually degrading the SNR gains expected at higher magnetic field strengths. As a coil is increased in physical dimension and/or frequency, its electrical circuit length increases. As its electrical length increases toward $\lambda/2$, the coil ceases to behave like a "coil" (RF field storage circuit) and begins to behave more like an "antenna" (RF field radiator). Coil builders experience these radiative losses as diminished Q and B_1 field, or as problematic "E-field coupling" when they tune a large coil to higher frequencies. Coil users experience these losses as increased RF power requirements for 90° pulse calibrations, as lower SNR, or as the lack of an available body coil. One remedy for radiation loss is to add more series capacitors, thereby dividing the voltage nodes of the circuit. This lumped-element approach to distributed circuit design quickly reaches its limits. Another approach is to build a coil by distributed circuit design using transmission line or TEM theory. Coil circuits incorporating flat or coaxial transmission line, stripline or microstrip, and resonant cavities or waveguides are examples of TEM circuits. In theory, the TEM circuit eliminates radiation loss. Therefore, the TEM volume coil design should be a good candidate for providing an efficient large volume transmit coil at the highest frequencies.

With the first NMR coil, a coaxial cavity resonator developed by Pound and Purcell 56 years ago at Harvard, the benefits of TEM design were realized (14a). Since then Schneider and Dullenkopf (15), Bridges (16), Röschmann (17), Barfuss et al. (18), and others have made use of transmission line principles, especially for the design of high-frequency coils. The optimized shielded birdcage design can also be viewed as a transmission line coil in which the foil strip rungs (striplines or center conductors) define a load-matched characteristic impedance with the shield (19,20). Barberi et al. (21) actively detuned such a shielded birdcage for use as a homogeneous transmitter at 4T. Modern TEM coil designs have achieved new levels of performance at unprecedented frequencies for human and other primate studies (22–30,45).

MATERIALS AND METHODS

The TEM transmit coil, together with its receivers, switches, and controls, comprises much of the RF front-end of a high-field system. The design, construction, and evaluation of the RF coils and supporting front-end equipment follow.

Detunable TEM Coil

The detunable TEM volume coil (first described by the author in U.S. patent application 60/135269; 1999) is schematized in Fig. 1. The detunable coil circuit consists of the coil body, the RF signal drive circuit, and the PIN diode detuning circuit for the coil. The materials and methods for constructing these components are explained in more detail below.

Coil Body

The coil was built according to a TEM design consisting of a segmented copper-foil cavity resonant with 24 capacitive line elements (13,26,35). See Figs. 2 and 3. The cavity measured 38 cm o.d. by 25 cm in length. The inside diameter of the coil delineated by the line elements was 32 cm. The high element count improved the peripheral *x-y* homogeneity of the coil. The resonance characteristics of this coil have been previously described (13,31,32). The coil was driven in quadrature and actively detuned with shunt PIN diodes bridging the line elements to the outside cavity wall, as in Fig. 1 (U.S. patent 60/135269) and Refs. 28 and
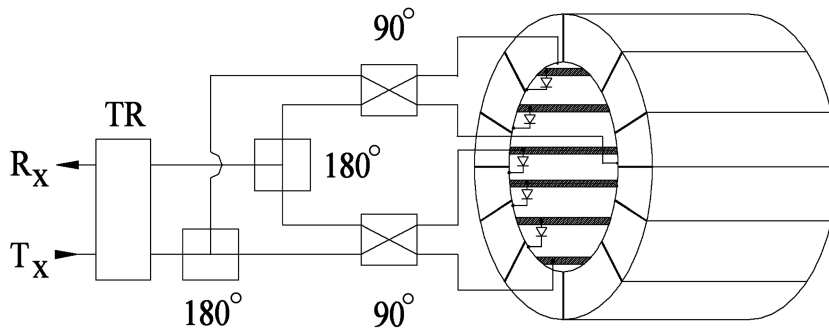
FIG. 1. The actively detuned TEM volume coil is shown. The coil is capable of operating in transmit and/or receive modes, and is actively detunable for operation with independent receiver coils. Included in the four-port drive circuit are a pair of 180° splitter/combiners, a pair of 90° hybrids, and a T/R switch.

29. Construction and evaluation details are explained in the following paragraphs.

Coil Cavity

Two definitions help to describe and clarify the integral cavity component of the TEM coil circuit, and to differentiate it from the "shield" often used with the birdcage coil design. A cavity is "a metallic enclosure inside which resonant fields may be excited." Further, a cavity resonator is "a space which is normally bounded by an electrically conducting surface and in which oscillating electromagnetic energy is stored; the resonant frequency is determined by the geometry of the enclosure." The TEM coil by definition, is a cavity resonator. By contrast, a shield is "a metallic covering placed around or between electric circuits to suppress the effects of undesired signals. . ." (33). While the birdcage shield was initially designed and applied at lower frequencies to perform the Faraday shielding function (20,34), it can have cavity-like properties and benefits for improving the efficiency of the birdcage and other coil designs at higher frequencies.

Both the birdcage shield and the TEM cavity must be segmented or slotted to sufficiently break up switched gradient-induced eddy currents. Viewing the birdcage with its end rings as a closed-ladder network of loops, the optimal birdcage shield is segmented in "thumbprint" patterns so as to not interrupt looping RF current patterns induced on the shield by the cage currents (20). The TEM coil, however, can be designed for negligible end-ring current. The significant current return path from the line elements in the TEM resonator is on the cavity wall, in the z direction. The current paths of the birdcage and the TEM coil are in this way fundamentally different, giving the two coil designs different resonance modes and performance properties. The optimal TEM cavity segmentation method is also different. The TEM cavity must be segmented in the z direction, from the front (head entry side), to the back wall of the cavity (Fig. 1). Any x or y component in the TEM cavity segmentation pattern interrupts or adds inductance to the return path circuit. A thumbprint design for the TEM cavity would therefore be suboptimal.

Connected slots were etched in the front, back, and cylindrical outside walls of the TEM cavity (Fig. 2). The slots were etched on two sides of a double-sided 5-μ–thick copper film deposited on a 12-μ–thick polyimide substrate (Sheldahl, Inc.). The slots on one side were overlapped by lands on the other side. The capacitive bridging thereby achieved between the segments provides low impedance to the RF currents and high impedance to the gradient-induced eddy currents between segments, improving the RF conduction efficiency and shielding qualities of the cavity. A similar effect has been achieved in other TEM head coils by capacitive bridging across the slots etched in a single-layer foil cavity. However, because there is little azimuthal RF current in the TEM cavity, the coil has been demonstrated to operate well in some cases without capacitive bridging between single-sided foil segments. The foil thickness was chosen to be the approximate RF skin depth at the desired frequency for added low-frequency eddy current attenuation (35).

The cylindrical inside wall of the coil cavity is composed of a plurality of conductive elements or "rungs" coaxial with the outside wall of the cavity. Whether in the form of striplines or coaxial members, these elements are often shortened and tuned by series capacitance. This capacitance can be added as lumped elements, or distributed over the element as shown in the Fig. 3. In the case of the stripline element, the capacitance is distributed be-
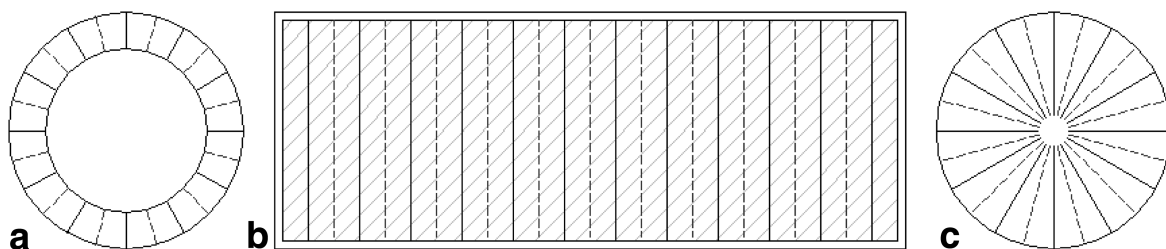

FIG. 2. Shown are the (**a**) open front wall, (**b**) cylindrical outside wall, and (**c**) (optionally) closed back wall of the TEM cavity. Solid and dotted lines mark the etched, nonconducting traces on each side of the double-sided, copper-clad, dielectric substrate. Overlapping conductive segments result. Twenty-four overlapping segments were etched on each side of the cavity wall for the coil built.
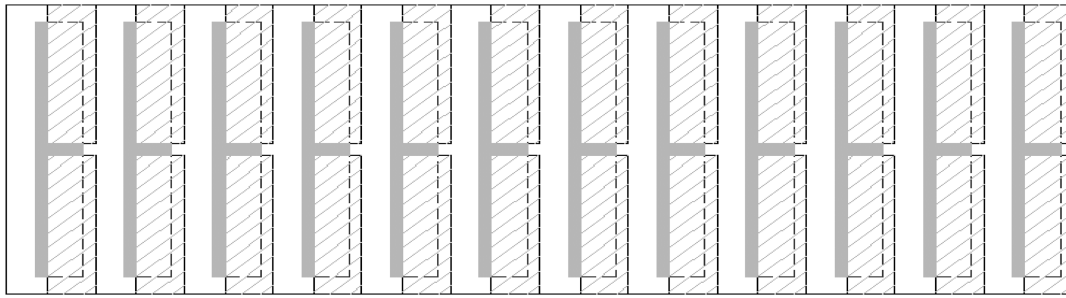
FIG. 3. The inside wall of the cavity comprised 24 capacitive line elements or "rungs" coaxial with the outside wall of the cavity. These elements may be coaxial, stripline, or double-sided, as shown. The parallel inside and outside walls form the coaxial or TEM cavity.

tween the cavity wall and the element across a dielectric layer of air, Teflon, or other material. The inside wall of the TEM cavity can be easily manufactured by etching the capacitive elements or striplines as shown on single- or double-sided, copper-clad, flexible circuit board (Rogers RT/Duroid). Alternatively, to improve E-field shielding the capacitive elements may be constructed as coaxial line sections with split center conductors (17). Both methods were employed in this study.

RF Drive Circuit

TEM transmit coils may be driven at two or four points (13,25,30) (Fig. 1). To circularly polarize the coil, two drive points can be reactively coupled to the coil elements at the $-45°$ and $+45°$ positions, or at the $135°$ and $225°$ positions relative to the bottom of the coil at $0°$. These drive points correlate coil symmetry to head symmetry. The phase of the RF drive signal must be shifted accordingly. For two-point drive, a quadrature hybrid may be used to accomplish the $90°$ phase shift between the two drive points. Four-point drive is often required to achieve best homogeneity for TEM coils of larger dimension and/or higher frequency. Body coils require four drive points, as do 7T head coils, for example (30). Four-point drive was achieved in this investigation by driving the $-45°$, $+45°$, $135°$, and $225°$ positions with RF signals divided and

phase-shifted accordingly. One $180°$, 3-dB power splitter fed a pair of $90°$ hybrids (QH-21N, KDI/Triangle) to accomplish the four-point transmit signal feed to the coil. Similarly, a $180°$ combiner recombined the signals received from the four-port coil's two quadrature hybrids (Fig. 1). Appropriately rated (>3 kW) T/R switches interfaced the common splitter and combiner ports to the transmit power amplifier and receive preamplifier, respectively (36).

PIN Detuning Circuit

To limit inductive coupling between the transmit coil and the receive coil placed within, the transmit coil must be detuned when the receive coil is tuned for signal reception; the receive coil must be detuned when the transmit coil is tuned for transmission. Both transmit and receive coil detuning was accomplished by using PIN diode circuits to change the circuit length or impedance of the coils.

In the TEM coil, PIN diodes (MA4Pk2002) were mounted in a shunt position connecting each of the coil's 24 line elements across a capacitance to the grounded cavity wall (Fig. 4). To detune the TEM coil, the diodes were forward biased with approximately 150 mA at 5 Vdc to short the elements to the cavity wall. When the diodes were reverse biased with -35 Vdc, the coil was tuned.

The PIN diode detuning circuit was selected to have a low loss characteristic while being rated to 4 kW peak
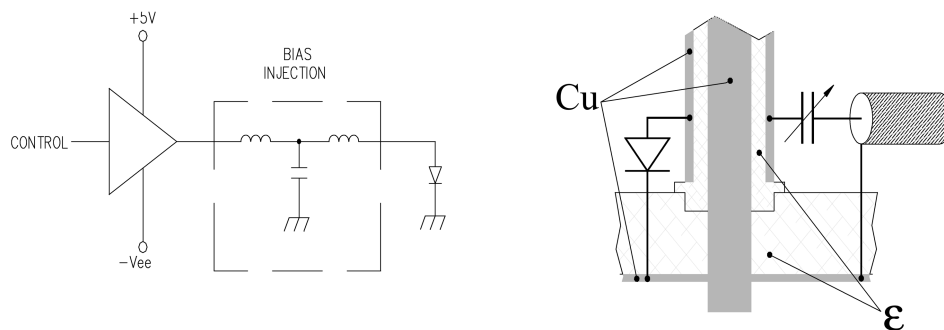

FIG. 4. Diagram of the basic diode driver for the TEM head coil. The TTL-controlled driver circuit with supplies is physically remote from the coil-embedded diodes, being located outside of the shielded room for the magnet. The diodes are attached to the coaxial elements for active detuning. When current is biased "on," the diode shorts the outer conductor of the coaxial line element to the grounded cavity wall of the coil. When the diode is voltage-biased "off," the connection is reopened with high impedance to restore the operational configuration of the tuned TEM coil. The RF blocking capacitance and inductance values used were 1 μF and 400 nH, respectively.
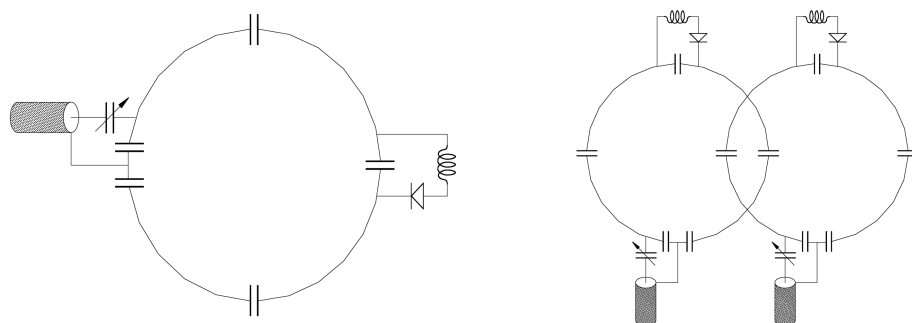
FIG. 5. The single- and double-looped surface coils used an active PIN diode trap tuned to the proton frequency to detune each surface coil during the volume coil transmit mode. These receive coils were etched from flexible circuit board material.

power at 170 MHz. The nonmagnetic diode demonstrated a sufficiently fast 10-μs switching speed. In shunt switch designs, the isolation and power dissipation are functions of the diodes' forward resistance. The PIN diode insertion loss, dependent on the diode capacitance, was not an important factor in this detuning application.

Parallel channels of twisted pair lines provided the voltage bias to each diode. In the case of a diode failure only one coil element would be affected, allowing safe coil function to continue, albeit with diminished RF efficiency and homogeneity. However, with 5 kV rating and high thermal capacity heat sinking, this robust design is largely immune to diode failure. The bias driver under NMR pulse sequence control turned the diodes off (high impedance) during transmit and on (conducting) during receive. The same bias electronics also provided independently controlled current pulses to detune the receive coil during transmit. A layer of polyethylene insulator material isolated the diode detuning voltages from any risk of subject contact. The measured level of decoupling between the transmit coil and a co-resonant surface coil receiver was used to determine the performance of the active PIN diode decoupling circuits.

Detunable Surface Coil

The receiver coils used were of standard single-loop linear and double-loop quadrature surface coil design (Fig. 5). The 8-cm linear and quadrature surface coil loops were built from copper tape or circuit boards and distributed (ATC 100E) capacitors. Designed for high power rating, these coils were used for T/R testing as well as receive-only operation. The surface coils were detuned with a resonant trap circuit using M/ACom MA4PK2000 diodes.

Coil Performance Evaluation

The performance of the actively detuned TEM head coil was measured on the bench and in the NMR experiment. The bench tests included measurement of the resonant frequency, unloaded and loaded coil quality factors (Q's), RF (B_1) field homogeneity, relative B_1 field gain (tuned and detuned), and the isolation between the TEM transmit coil and the surface coils within. The NMR measurements included the 90° pulse calibration measurement for the volume coils, B_1 field distribution for volume and surface coils, SNR for volume and surface coils used separately and together, and the signal-to-ghost ratio (SGR) measurement for the segmented TEM volume coil.

Bench Measurements

The bench measurements were made using a calibrated Hewlett-Packard 4396A network analyzer together with an 85046A "S" parameter test set by the same company. Both unloaded and loaded coil measurements were made, the load being a 3-L, 25-cm-long cylindrical bottle filled with .5 N NaCl solution. The TEM volume coil and surface coils were both verified to be tuned to the 169.7 MHz Larmor frequency for our 4T magnet. The S_{11} and S_{22} network reflection measurements were used to verify tuning and impedance matching for the coils used. For example, S_{11} was used to determine the tuned frequency and impedance match of the loaded and unloaded, circularly polarized TEM coil at the transmit signal port of the quadrature hybrid feeding the coil. The S_{22} measurement determined the tuned frequency and match at the receive port of the hybrid. The S_{12}, or reciprocal S_{21} network transmission measurements were used to measure the isolation between the transmit and receive ports of the quadrature hybrid feeding the circularly polarized TEM coil. The B_1 gain is defined here as the coil center field magnitude per unit RF signal input to the coil. B_1 gain and field contour measurements were made by S_{12} and S_{21}, respectively, by driving the coil at the transmit and then the receive ports while receiving the B_1 field component at the coil center with a 1.5-cm-diameter shielded magnetic dipole field probe. The Q was measured from the S_{11} parameter as the ratios of the design center frequency over the 3-dB bandwidths for the unloaded and head phantom loaded coil. The coupling and decoupling magnitudes between the surface coil and the TEM volume coil were measured by S_{12}, transmitting with the volume coil and receiving with the surface coil, and vice versa. Finally, the switching times of the PIN detuning devices driven by an HP 3245A universal source were measured with an HP54825A, four-channel, 500-MHz digitizing oscilloscope. These bench measurements are included in the Results section.

NMR Measurements

In the magnet, the coil was first tested in the passive T/R imaging mode. The RF power requirement, B_1 homogeneity, and SNR for the detunable coil were compared to the performance of passive TEM and shielded birdcage head coils used at 4T. The detunable coil's performance was then tested as a transmit-only coil together with a detunable, receive-only surface coil. These results from the transmit and receive coils together were then compared to
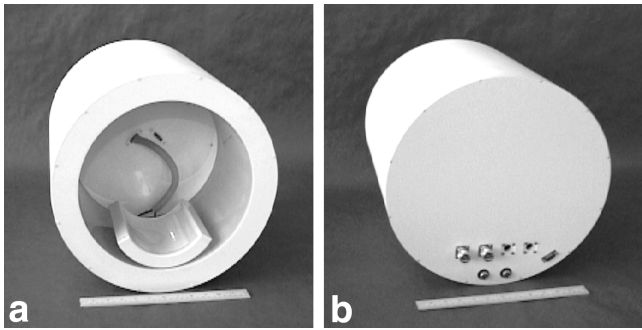
FIG. 6. Shown is the detunable TEM transmit coil with a local receiver coil built for the study. Front and back views are visible in **a** and **b**, respectively.

the images of a passive transceiver (transmit and receive) surface coil. After the basic RF power, B_1, and SNR data were collected for the transmit and receive coil combinations, the detunable TEM coil was evaluated by its application to human imaging.

Calibration of RF Source

The RF power requirements to achieve 90° flip angles for the detunable TEM volume coil and comparison coils were calibrated for the head using a projection of the transaxial center-slice signal intensity. These measurements were performed with a spin-echo sequence in which the voltage of the second (refocusing) pulse was set to twice the first (excitation) pulse. The RF power of these pulses was simultaneously incremented by 1-dB steps. As the power was incremented, full recovery of the longitudinal magnetization (TR = 10 s) was allowed between consecutive acquisitions.

TEM Coil Coupling to Surface Coils

After the isolation between the transmit and receive coils was tested on the bench, coil decoupling was verified by phantom imaging. Inadequate detuning of a surface coil could be visualized as nonuniform image intensity due to local variations in flip angles resulting from residual currents induced in the surface coil during transmit. The local B_1 field from these induced currents would be superimposed on the otherwise homogeneous transmit field. Inadequate detuning of the transmit coil would be evident as

increased noise coupling into the loaded surface coil receiver.

SNR

To measure the SNR for the coils of this study, density-weighted gradient-echo images were acquired from the head using the following parameters: TR/TE = 5000 ms/5 ms, NEX = 1, receiver bandwidth = 100 kHz, slice thickness = 5 mm with a 2-ms Gaussian-shaped pulse, FOV = 24 cm × 22 cm, matrix size = 256 × 256. For whole-head images acquired for SNR comparisons from the volume coils only, the RF power was determined by the 90° flip-angle calibration in a central transaxial slice from the head. For surface coil comparisons the RF power was calibrated for the T/R surface coil, and for the combined transmit coil and surface coil receiver such that the 90° flip angle was optimized within the first 2 cm depth into the occipital lobe.

Spin-Echo Imaging

Multislice spin-echo images provided for B_1-sensitive observation and comparison of human head images acquired with the detunable TEM coil, the surface coils, and the T/R volume coils. Modified driven equilibrium Fourier transform (MDEFT) in a multislice spin-echo sequence (1,39) was used to acquire T_1-weighted anatomical images with the following parameters: TR/TE = 1500 ms/13.5 ms, NEX = 2, receiver bandwidth = 48 kHz, four slices, thickness = 3.5 mm with 4.5-ms five-lobe sinc-shaped pulses for excitation and refocusing, 78-ms frequency-swept (chirp) inversion, sagittal FOV = 30 × 24 cm, axial FOV = 24 × 22 cm, and matrix size = 256 × 256.

Adiabatic Imaging

Arguments can be made for adiabatic T/R imaging with a surface coil only for some applications, in lieu of a homogeneous transmit coil. To evaluate this alternative, imaging measurements were performed with surface and volume coils using a double spin-echo sequence based on B_1-insensitive adiabatic pulses (40). This sequence used a 4-ms nonselective adiabatic half-passage and two 8-ms hyperbolic secant pulses for excitation and slice-selective refocusing, respectively (6,40). The RF power levels used for the volume coil and the surface coil transmission were separately adjusted. Imaging parameters were: TR/TE =

Table 1
Volume Coil Specifications and Performance at 4T

| Volume coil with slotted shield	Length	I.D.	FOV	Q_u/Q_1	$\frac{B_1gain_u}{B_1gain_1}$	90° head	15 cm DSV, B_1 homogeneity	SNR head	SGR head
Passive birdcage, 2 ends open	21 cm	27 cm	whole head	210/40	$\frac{-26\ dB}{-34\ dB}$	$\frac{305\ \mu sec}{1\ kW}$	<1 dB var. unloaded	85 center	192
Passive TEM, 1 end closed	21 cm	27 cm	whole head	800/65	$\frac{-21\ dB}{-30\ dB}$	$\frac{255\ \mu sec}{1\ kW}$	<1 dB var. unloaded	115 center	180
Active TEM, 1 end closed	25 cm	32 cm	whole head	730/90	$\frac{-27\ dB}{-32\ dB}$	$\frac{300\ \mu sec}{1\ kW}$	<1 dB var. unloaded	89 center	228
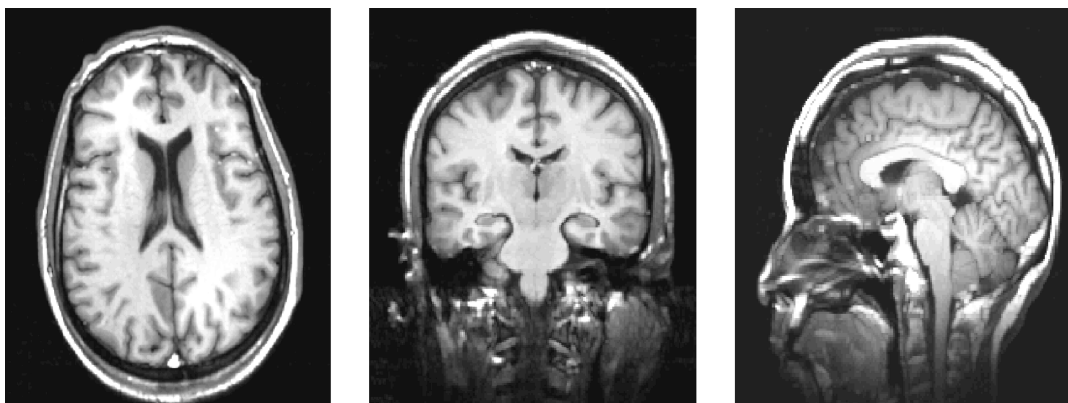
FIG. 7. The center-slice transaxial, coronal, and sagittal images shown were acquired using the multislice spin-echo MDEFT sequence described in Methods. The images were obtained by using the detunable TEM coil alone in the T/R mode. A detuned surface coil receiver was adjacent to the occipital lobe during image acquisitions. Coupling between the volume coil and the detuned surface coil is not evident.

2500/50 ms, NEX = 2, FOV = 18 × 18 cm², thk = 3.5 mm, and matrix size = 256 × 256.

Echo-Planar Imaging (EPI)

Image ghosting is an artifact often visible in echo-planar images acquired with shielded coils. This ghosting results from switched gradient induced eddy currents in the cavity and shield components of volume coils. The SGR was therefore measured from phantom images acquired with the volume coils used in the study. Additionally, an example functional MRI (fMRI) study was performed using a surface coil only, and then a surface coil receiver with the TEM transmit coil to obtain maps of increased brain activity resulting from flashing LEDs. EPI data acquisition used eight segments (256 × 256) with an FOV of 20 × 20 cm², thk = 6 mm, and TR/TE = 1000 ms/25ms.

RESULTS AND DISCUSSION

Coil Performance

The results from the evaluation and application of the detunable TEM coil with surface coils are tabulated and discussed in this section. Figure 6 shows the TEM transmit coil with a surface coil receiver.

Volume Coils

The actively detunable 32-cm-i.d. TEM coil was first tested in the T/R head coil mode and compared to two smaller-diameter (27 cm i.d.) passive T/R head coils in the lab, a high-pass shielded birdcage, and a TEM resonator (Table 1). Three planes of spin-echo head images were acquired with the T/R coil of Fig. 6 are shown in Fig. 7. As expected, the smaller 27-cm TEM coil was more efficient, with higher Q, relative B_1 gain, and lower 90° power requirements than the 32-cm TEM coil. While the larger coil was loaded by the head and neck compared to the head only for the smaller coil, the loaded Q ratios indicate that the 27-cm TEM coil was more strongly coupled to the load. The higher "fill factor" for the smaller coil explains this finding. However, the 32-cm TEM coil performed well by conventional standards, comparing favorably to the 27-cm

shielded birdcage in terms of B_1 and SNR measurements. These results are consistent with previous reports (28,29). The EPI SGR was measured as an indicator of the eddy currents induced in the conductive surfaces of the coils. The SGR was highest (best) for the larger, detunable coil because its conductive walls were located further from the NMR sample.

In addition to image ghosting, switched gradient-induced eddy currents in the coil's cavity wall were observed to generate ohmic heating, especially in unslotted shields or cavities. Table 2 compares fluoroptically measured temperature rises vs. time for slotted and unslotted coil cavities. The cavity wall temperatures recorded in this table were induced by delivery of a continuous trapezoidal gradient waveform with single-shot EPI gradients (matrix = 64 × 64, amplitude = 3.5 G/cm, TR = 100 ms) applied to head coils by a close-fitting 38-cm-i.d. gradient coil set (Magnex Scientific, Oxford, UK). Slotting a cavity or a shield is clearly necessary for limiting the gradient-induced eddy currents and consequent heating.

Surface Coils

Surface coils were tested and compared as stand-alone T/R coils and as receive-only coils for use with the actively detunable TEM volume coil. For this study, 8-cm-diameter surface coils were prepared accordingly for use in transmit and receive modes. The SNR values within one coil radius (3 cm tissue + 1 cm spacing) of the single-looped receivers were measured to be higher by nearly a factor of 4 than the SNR measured with the head coil from the same occipital cortex ROI. The SNR from the passive T/R surface coil had

Table 2

Temperature Measurements of RF Heating in Unslotted and Slotted TEM Cavity

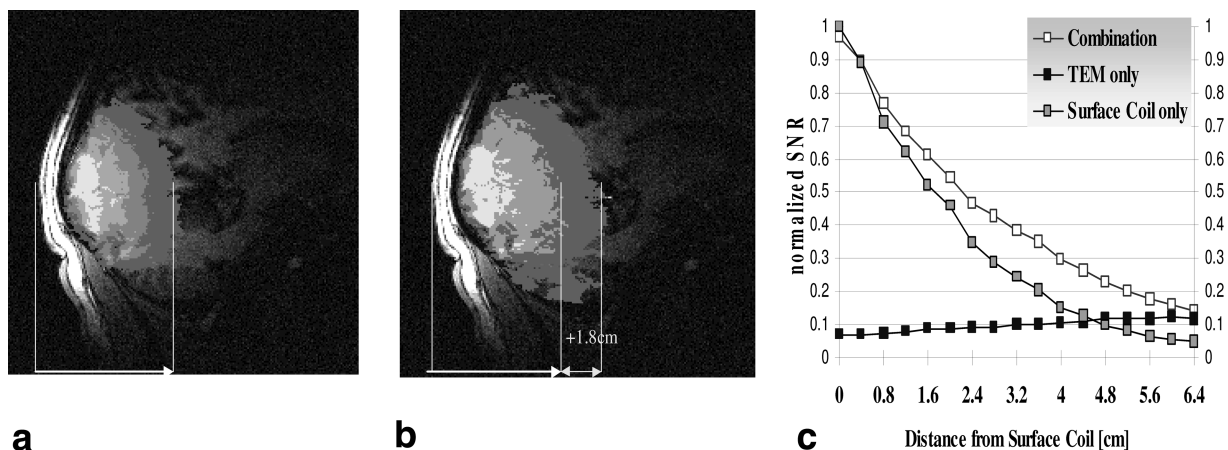|	δT/min unslotted cavity, °C	δT/min slotted cavity, °C
x-readout	2.5	0.4
y-readout	3.9	0.3
z-readout	1.5	0.4

FIG. 8. **a:** SNR maps generated from T_2^*-weighted GE-EPI images acquired with an 8-cm T/R surface coil only. **b:** The same SNR contours obtained with a detunable TEM transmit coil used together with a detunable 8-cm surface coil receiver. For a given SNR value, the FOV is extended about 30% deeper in **b** than in **a**, as marked by verticle lines in these figures. **c:** SNR vs. tissue depth for the T/R TEM volume coil only, the T/R surface coil only, and for the combined use of the TEM volume coil and the surface coil. The RF power requirement was calibrated for each coil or combination such that the 90° flip angle occurred within a 2-cm depth in the visual cortex.

a value similar to that using the receive-only coil, within a narrow range corresponding to the 90° ± spin angle excitation, less than one radius from T/R the coil. The approximate quadrature orientation and reception from the paired loops improved the SNR by a factor of 5 times that of the T/R head coil alone for the superficial ROI. These results were expected, and explain why surface coils are used for localized MRI. The limited range and inhomogeneity of surface coils are often tolerated for these SNR improvements. By combining the volume coil excitation with surface coil receivers, however, it is possible to extend the range and uniformity of this SNR improvement.

Volume and Surface Coils Combined

The limited homogeneity and FOV for surface coils, and the limited SNR for the larger TEM volume coil can be partially compensated by using the two coil types together. Homogenous excitation is achieved with the volume coil, while the surface coil facilitates sensitive signal detection. When the surface and volume coils were combined in this study, the surface coil received high SNR signal from an extended, homogeneously excited FOV (Fig. 8). When the surface coil was used for both transmit and receive operations, the high SNR FOV was limited compared to the

SNR that can be achieved with spatially uniform excitation. The SNR for the receive-only surface coil used together with the TEM transmit coil extended to a larger FOV, compared to the T/R surface coil used alone. This observation held true even when adiabatic pulse sequences are employed with a T/R surface coil (Fig. 9). Similar results have been demonstrated for more conventional bridcage coils and at lower field strengths (21,37,38). The actively detuned TEM coil now makes independent transmit and receive coil operation possible to 7T and beyond for head and body applications (30,41,42,45).

Coil Applications

The detunable head coil and surface coils were evaluated for anatomical and functional imaging and spectroscopy of human brain applications at 4T. The following results from these applications demonstrate the utility of the actively detunable TEM coil for high-field NMR.

Imaging

The 32-cm-i.d. detunable TEM coil was used as a transmit and receive imaging coil to acquire whole-head images in which the SNR and homogeneity were comparable to images

FIG. 9. Adiabatic image acquisitions were compared using (**a**) inhomogeneous excitation and reception with a surface coil only, and (**b**) homogeneous excitation from the detunable TEM volume coil with a surface coil receiver. Even with the adiabatic approach, the use of a transmit volume coil with a local receiver extended the sensitive volume of the active receive-only surface coil beyond the range of the passive T/R surface coil.
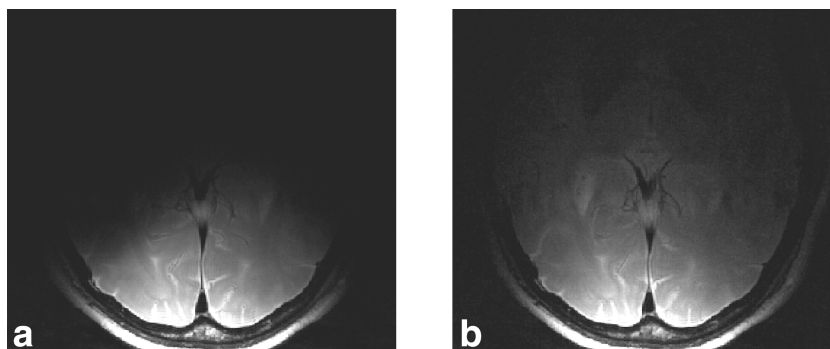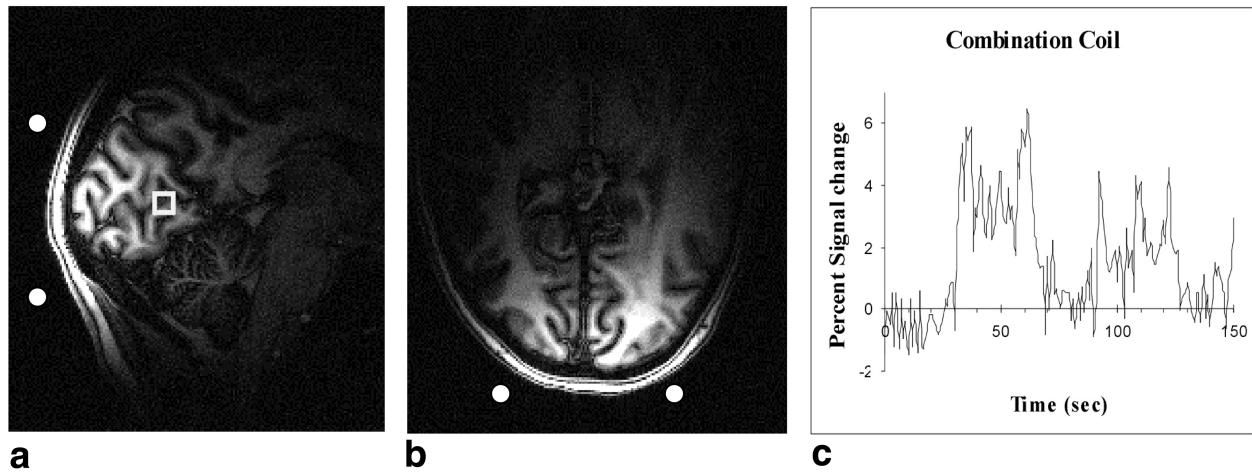
FIG. 10. T_1-weighted anatomic images of the primary visual area were acquired using a 256 × 256 turbo-fast low-angle shot (FLASH) sequence with a homogeneous transmit coil actively decoupled (>50 dB) from an 8-cm surface coil used during signal reception only. An activation time course was measured from the 4-cm-deep ROI marked in the visual cortex along the calcarine sulcus (**c**). The visual stimulation was turned on during imaging at 25–60 s and 90–115 s.

acquired with a 27-cm shielded birdcage coil at 4T (Table 1, Fig. 7). Such images provide for convenient scout images and landmarks for superimposed CSI and fMRI results obtained from localized regions with dedicated receivers.

Spectroscopy

The actively detuned TEM volume coil has been used previously to uniformly excite large ROIs from which high-SNR localized spectra have been acquired with surface coil receivers. The TEM volume coil has also been dual tuned for proton decoupling experiments and other multinuclear studies (13).

fMRI

To demonstrate and evaluate the detunable TEM volume coil and surface coil combination in an fMRI application, EPI measurements were acquired from a volunteer performing a simple visual stimulation task using flashing LEDs. In activation maps with the same confidence thresholds, it was possible to detect activation deeper in the visual cortex along the calcarine sulcus (more distant from the surface coil) when using the TEM volume coil transmit plus surface coil receive technique, as opposed to transmitting and receiving with the surface coil alone. This is illustrated by the time course observed for a ROI distant from the surface coil, 4–5 cm deep in the visual cortex (Figs. 10 and 11). An increase in the signal intensity during visual stimulation was clearly observed with the volume coil plus surface coil combination (Fig. 10), but not with the T/R surface coil alone (Fig. 11). The data were corrected for respiration and cardiac fluctuations, using an algorithm that is highly dependent on SNR (43). Therefore, better suppression of physiological noise may have
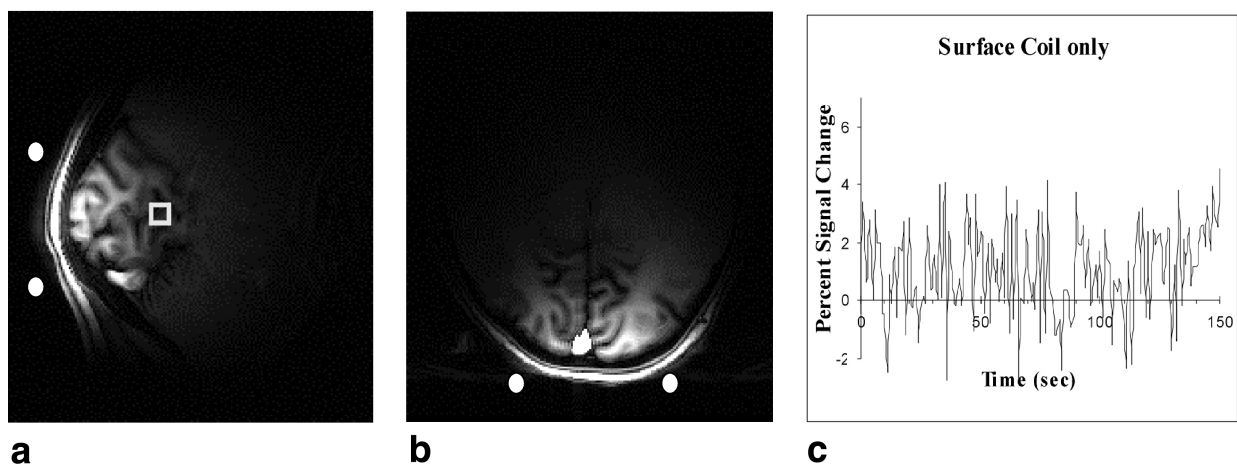

FIG. 11. Images acquired with the same parameters as in Fig. 10, but with an 8-cm passive, T/R surface coil only. The images show the limited FOV for the passive T/R surface coil as compared to Fig. 10, in which the same surface coil was used in receive-only mode together with a volume transmit coil. The lack of detectable activation in **c** shows that the ROI of Fig. 10 is out of range for the surface coil alone.

slightly exaggerated the higher SNR in Fig. 10 as compared to Fig. 11. At the deep visual cortex ROI shown, the SNR appears to have increased by approximately threefold for the receive-only surface coil compared to the T/R head coil alone, and by nearly twofold compared to the SNR for the T/R surface coil. The volume coil transmit with surface coil acquisition measured higher SNR over an extended FOV, as demonstrated in Fig. 8.

Other fMRI experiments produced results similar to those above, taking advantage of the benefits of homogeneous transmission and high SNR reception. In addition to the GE blood oxygen level-dependent (BOLD) fMRI examples above, there are fMRI approaches that require uniform inversion over the entire head. Two such approaches benefiting from homogeneous excitation are cerebral blood flow (CBF)-based fMRI using FAIR and spin-echo BOLD fMRI, in which a 180° refocusing pulse is required over the entire FOV. Acquiring images of CBF and CBF-based activation in the brain requires uniform inversion in a slice as well as over a large volume, at least the entire head, and preferably over the head and neck. This requirement cannot be fulfilled with surface coils alone, even with adiabatic inversion pulses. Using the large TEM resonator for transmitting while receiving with the surface coil becomes an ideal approach for obtaining high-SNR CBF maps or CBF-based fMRI maps. Similarly, spin-echo BOLD fMRI is ideally performed using the separate transmit and receive coil system when the SNR of the surface coil is desired (44).

CONCLUSIONS

The objective of this study was to realize further gains in SNR and protocol versatility for neuroimaging at the highest field strengths generally available. This goal was accomplished by developing an efficient transmit coil plus receive coil system for use at 4T. The detunable TEM coil was shown to provide an efficient body coil substitute for head imaging applications. NMR studies requiring uniform excitation and extended-field, high-SNR reception will benefit from the use of this coil. Similarly, homogeneous excitation allows the use of a smaller, more efficient surface coil receiver for SNR improvement from a given ROI. The detunable TEM head coil has been used together with detunable surface coils to enhance high-resolution anatomical, spectroscopic, and functional imaging at 4T. The detunable TEM volume coil reported has been extended to body imaging at 4T, to head imaging at 7T, and has demonstrated efficient performance to 343 MHz (8T) in bench studies (45).

REFERENCES

1. Ugurbil K, Garwood M, Ellermann J, Hendrich K, Hinke R, Hu X, Kim S-G, Menon R, Merkle H, Ogawa S. Imaging at high magnetic fields: initial experiences at 4T. Magn Reson Q 1993;9:259–277.
2. Ugurbil K, Hu X, Chen W, Zhu X-H, Kim SG, Georgopoulos G. Functional mapping in the human brain using high magnetic fields. Phil Trans R Soc Lond B 1999;354:1195–1213.
3. Pan JW, Vaughan JT, Kuzniecky RI, Pohost GM, Hetherington HP. High resolution neuroimaging at 4.1T. Magn Reson Imaging 1995;13:915–921.
4. Hetherington H, Kuzniecky R, Pan J, Mason G, Morawetz R, Harris C, Faught E, Vaughan T, Pohost G. Proton nuclear magnetic resonance spectroscopic imaging of human temporal lobe epilepsy at 4.1 T. Ann Neurol 1995;38:396–404.
5. Gruetter R, Seaquest ER, Kim SW, Ugurbil K. Localized in vivo 13C NMR of glutamate metabolism in the human brain. Initial results at 4 Tesla. Dev Neurosci 1998;20:380–388.
6. Conolly S, Glover G, Nishimura D, Macovski A. A reduced power selective adiabatic spin-echo pulse sequence. Magn Reson Med 1991;18:28–38.
7. Conolly S, Nishimura D, Macovski A. A selective adiabatic spin-echo pulse. J Magn Reson 1989;83:324–334.
8. de Graaf RA, Nicolay K, Garwood M. Single-shot, B_1-insensitive slice selection with a gradient-modulated adiabatic pulse, BISS-8. Magn Reson Med 1996;35:652–657.
9. Hwang T-L, van Zijl PCM, Garwood M. Broadband adiabatic refocusing without phase distortion. J Magn Reson 1997;124:250–254.
10. Duensing GR, Peterson DM, Wolverton BL, Fitzsimmons JR. Transceive phased array for imaging at 3.0T. In: Proceedings of the 6th Annual Meeting of ISMRM, Sydney, Australia, 1998. p 441.
11. Hoult DI, Lauterbur PC. The sensitivity of the zeugmatographic experiment involving human samples. J Magn Reson 1979;34:425.
12. Hoult DI, Chen CN, Sank VJ. The field dependence of NMR imaging. II. Arguments concerning optimal field strength. Magn Reson Med 1986;3:730.
13. Vaughan JT, Hetherington HP, Harrison JG, Otu JO, Pan JW, Pohost GM. High frequency volume coils for clinical NMR imaging and spectroscopy. Magn Reson Med 1994;32:206–218.
14. Libby LL. Special aspects of balanced shielded loops. In: Proceedings of IRE and Waves and Electrons, 1945. p 641–646.
14a. Purcell EU, Torrey HC, Pound RV. Resonance absorption by nuclear magnetic moments in a solid. Phys Rev 1946;69:37–38.
15. Schneider HJ, Dullenkopf P. Slotted tube resonator: a new NMR probe head at high observing frequencies. Rev Sci Instrum 1977;48:68.
16. Bridges JF. Cavity resonator with improved magnetic field uniformity for high frequency operation and reduced dielectric heating in NMR imaging devices. U.S. patent 4,751,464; 1988.
17. Röschmann PK. High-frequency coil system for a magnetic resonance imaging apparatus. U.S. patent 746,866; 1988.
18. Barfuss H, Fischer H, Hentschel D, Ladebeck R, Oppelt A, Wittig R, Duerr W, Oppelt R. In vivo magnetic resonance imaging and spectroscopy of humans with a 4T whole-body magnet. NMR Biomed 1990;3:31.
19. Hayes CE, Edelstein WA, Schenck JF, Mueller OM, Eash M. An efficient highly homogeneous radiofrequency coil for whole-body NMR imaging at 1.5T. J Magn Reson 1985;63:622–628.
20. Roemer PB, Edelstein WA. Double-sided RF shield for RF coil contained within gradient coils of NMR imaging device. U.S. patent 4879515; 1989.
21. Barberi EA, Gati JS, Rutt BK, Menon RS. A transmit-only/receive-only (TORO) RF system for high field MRI/MRS applications. Magn Reson Med 2000;43:284–289.
22. Vaughan JT, Otu JO, Hetherington HP, Noa P, Pohost GM. A high frequency tuned resonator for clinical NMR. In: Proceedings of the 11th Annual Meeting of SMRM, Berlin, 1992. p 279.
23. Vaughan JT. High frequency volume coils for nuclear magnetic resonance applications. U.S. patent 5,557,247; 1996.
24. Vaughan JT, Garwood M, Merkle H, Adriany G, Uckun FM, Ugurbil K. First 9.4T homogeneous head imaging of a monkey. In: Proceedings of the 82nd Annual Meeting of RSNA, Chicago, 1996. p 292.
25. Zhang N, Roos MS, Vaughan JT, Wong STS, Budinger TF. Head coil B_1 field homogeneity and SNR performance at 8–10T. In: Proceedings of the 4th Annual Meeting of ISMRM, New York, 1996. p 252.
26. Vaughan JT. An improved volume coil for high field MRI. In: Proceedings of the 7th Annual Meeting of ISMRM, Philadelphia, 1999. p 167.
27. Robitalle P-ML, Abduljalil AM, Kangarlu A, Zhang X, Yu Y, Burgess R, Bair S, Noa P, Yang L, Hui S, Palmer B, Jiang Z, Chakeres DM, Spigos D. Human magnetic resonance imaging at 8T. NMR Biomed 1998;11:263–265.
28. Ledden PJ, Wald LL, Vaughan JT. A volume coil transmit, surface coil receive system for brain imaging at 3T. In: Proceedings of the 7th Annual Meeting of ISMRM, Philadelphia, 1999. p 168.

29. Adriany G, Yacoub E, Hu X, Garwood M, Merkle H, Chen W, Kim SG, Andersen P, Ugurbil K, Vaughan JT. A detunable TEM transmit coil for 4T fMRI and spectroscopy. In: Proceedings of the 8th Annual Meeting of ISMRM, Denver, 2000. p 145.

30. Vaughan JT, Garwood M, Collins CM, Liu W, DelaBarre L, Adriany G, Andersen P, Merkle H, Goebel R, Smith MB, Ugurbil K. 7T vs. 4T: RF power, homogeneity, and signal-to-noise comparison in head images. Magn Reson Med 2001:46:24−30.

31. Röschmann PK. Analysis of mode spectra in cylindrical N-conductor transmission line resonators with expansion to low-, high-, and band-pass structures. In: Proceedings of the 3rd Annual Meeting of ISMRM, Nice, France, 1995. p 1000.

32. Tropp J, Vaughan JT. The prospects for systematic design of TEM resonators. In: Proceedings of the 7th Annual Meeting of ISMRM, Philadelphia, 1999. p 421.

33. Graf F. Modern dictionary of electronics, 6th ed. Indianapolis: Howard W. Sams & Co; 1991. 143 p.

34. Shen GX. Double-sided stripline RF shield. In: Proceedings of the 11th Annual Meeting of SMRM, Berlin, 1992. p 4048.

35. Vaughan JT. Radiofrequency coils for imaging and spectroscopy. U.S. patent 5,886,596; 1999.

36. Vaughan JT, Haupt DN, Noa PJ, Vaughn JM, Pohost GM. RF front end for a 4.1 Tesla clinical NMR spectrometer. IEEE Trans Nucl Sci 1995; 42:1333−1337.

37. Boskamp EB. Improved surface coil imaging in MR: decoupling of the excitation and receiver coils. Radiology 1985:449−452.

38. Edelstein WA, Hardy C, Mueller O. Electronic decoupling of surface-coil receivers for NMR imaging and spectroscopy. J Magn Reson 1986; 67:156−161.

39. Tannús A, Garwood M. Reducing the RF power requirements of mul-tislice imaging using a single adiabatic frequency swept inversion pulse. In: Proceedings of the 4th Annual Meeting of ISMRM, New York, 1996. p 362.

40. Schupp DG, Merkle H, Ellermann JM, Ke Y, Garwood M. Localized detection of glioma glycolysis using edited ^{1}H MRS. Magn Reson Med 1993;30:18−27.

41. Vaughan JT, Hetherington HP, Pohost GM. A high frequency body coil for clinical NMR. In: Proceedings of the 2nd Annual Meeting of ISMRM, San Francisco, 1994. p 1113.

42. Vaughan T, Adriany G, Ugurbil K. High frequency RF body coil. In: Abstracts of Minnesota Workshops on High Field MR Imaging and Spectroscopy, Minneapolis, 2001. p 57−59.

43. Hu X, Le TH, Parrish T, Erhard P. Retrospective estimation and correction of physiological fluctuation in functional MRI. Magn Reson Med 1995;34:201−212.

44. Duong T, Yacoub J, Hu X, Adriany G, Merkle H, Andersen P, Vaughan JT, Ugurbil K, Kim SG. Diffusion-weighted BOLD fMRI at 4 and 7 Tesla: evaluation of micro- versus macrovascular contributions. In: Proceedings of the 9th Annual Meeting of ISMRM, Glasgow, Scotland, 2001. p 1253.

45. Vaughan JT, Adriany G, Bolinger L, Waks M, DelaBarre L, Garwood M, Andersen P, Ugurbil K. A body coil for high field MR. In: Proceedings of the 10th Annual Meeting of ISMRM, Honolulu, 2002.